RSC Advances

PAPER

View Article Online
View Journal | View Issue



Cite this: *RSC Adv.*, 2025, **15**, 15806

# A novel approach for the fabrication of SERS substrates based on 3D urchin-like $TiO_2$@Gr–AuNPs architecture

Nguyen Thi Huyen,[ab] Le Thi Quynh Xuan,[a] Tran Ai Suong Suong,[c] Cao Thi Thanh,[a] Pham Van Trinh,[a] Nguyen Van Tu,[a] Nguyen Thu Loan,[a] Luong Truc Quynh Ngan,[a] Pham Thanh Binh,[a] Cao Thi Linh Huong,[d] Dao Nguyen Thuan,[a] Vu Xuan Hoa,[e] Nguyen Van Hao,[e] Nguyen Van Quynh,[d] Hiroya Abe[f] and Nguyen Van Chuc *[ab]

3D urchin-like titanium dioxide@graphene–gold nanoparticles (UT@Gr–AuNPs) architectures with a core@shell structure of UT@Gr were successfully synthesized on silicon substrates *via* thermal chemical vapor deposition (CVD) technique using sodium deoxycholate surfactant (SDC) as a carbon source, followed by depositing AuNPs onto the surface of UT@Gr *via* a cold plasma (CP) process. The as-prepared samples were characterized by scanning electron microscopy (SEM), transmission electron microscopy (TEM), Raman, X-ray diffraction (XRD), energy-dispersive X-ray spectroscopy (EDS), and ultraviolet-visible (UV-vis) spectroscopy. Thanks to the hot spots created by the AuNPs onto the surface of UT@Gr, the UT@Gr–AuNPs SERS substrates show significantly enhanced SERS sensitivity to detect hazardous pollutants and pesticide residue substances, *e.g.*, rhodamine 6G (R6G) and malathion with a low detection limit (LOD) of about $5.86 \times 10^{-11}$ M and $2.87 \times 10^{-8}$ M, respectively. Moreover, these SERS substrates prepared in this study effectively enable *in situ* SERS monitoring of the R6G and rhodamine B (RhB) photodegradation reaction and self-cleaning performance under ultraviolet light (UV, 254 nm) irradiation.

Received 28th March 2025
Accepted 7th May 2025

DOI: 10.1039/d5ra02160j

rsc.li/rsc-advances



## 1. Introduction

Surface-enhanced Raman scattering (SERS) is an ultrasensitive tool used for quickly detecting traces of toxic substrates and pesticide residues in environments, agricultural products, and foods.[1–6] The SERS signal enhancement is known as electromagnetic enhancement (EM) and chemical enhancement (CM). The EM comes from hot spots in plasmonic metallic nanostructures with the intensity of the electromagnetic field on corrugated surfaces of noble metals, such as gold (Au),[7] silver (Ag),[1,4–6] copper (Cu),[8] palladium (Pd),[9] platinum (Pt),[10] and rhodium (Rh).[11] The CM is due to the charge transfer (CT) between analyte molecules and the SERS substrate surface.[12] Various SERS substrate types with high sensitive based on nanostructured noble metals have been fabricated by methods such as vapor deposition,[7,13] chemical reduction,[3,14–16] electron beam lithography,[17] nanoimprint lithography,[18,19] and ion-irradiation.[20] However, these SERS substrate types have limitations in terms of their reusability due to difficulty in removing the analyte molecules from the SERS substrate surface. Therefore, it is essential to develop the SERS substrate types that ensure both sensitivity and reusability.

In recent years, the titanium dioxide ($TiO_2$) semiconductor material combined with noble metals has been widely used as SERS substrates and photocatalysts on the degradation of various organic molecules. The combination of $TiO_2$ material with noble metals can efficiently separate photogenerated electrons from holes and decrease the electron–hole recombination rate, improve the CT efficiency and therefore enhance the SERS signals. Besides, the combination of $TiO_2$ with noble metals can also improve the self-cleaning and recycling ability of SERS substrates through photocatalytic degradation in the presence of visible or ultraviolet (UV) light irradiation.[21–24] With a large surface area, high carrier mobility, outstanding CM enhancement, and good fluorescence quenching ability, graphene material has also been used as a good SERS substrate.[25,26] Therefore, the combination of $TiO_2$ and graphene with

[a]*Institute of Materials Science, Vietnam Academy of Science and Technology, 18 Hoang Quoc Viet, Cau Giay, Hanoi, Vietnam. E-mail: chucnv@ims.vast.vn*
[b]*Graduate University of Science and Technology, Vietnam Academy of Science and Technology, 18 Hoang Quoc Viet, Cau Giay, Hanoi, Vietnam*
[c]*VNU University of Engineering and Technology, 144 Xuan Thuy, Cau Giay, Hanoi, Vietnam*
[d]*University of Science and Technology of Hanoi, Vietnam Academy of Science and Technology, 18 Hoang Quoc Viet, Cau Giay, Hanoi, Vietnam*
[e]*Institute of Science and Technology, TNU-University of Sciences (TNUS), Tan Thinh Ward, Thai Nguyen City, Vietnam*
[f]*Joining and Welding Research Institute, Osaka University, Osaka 5670047, Japan*

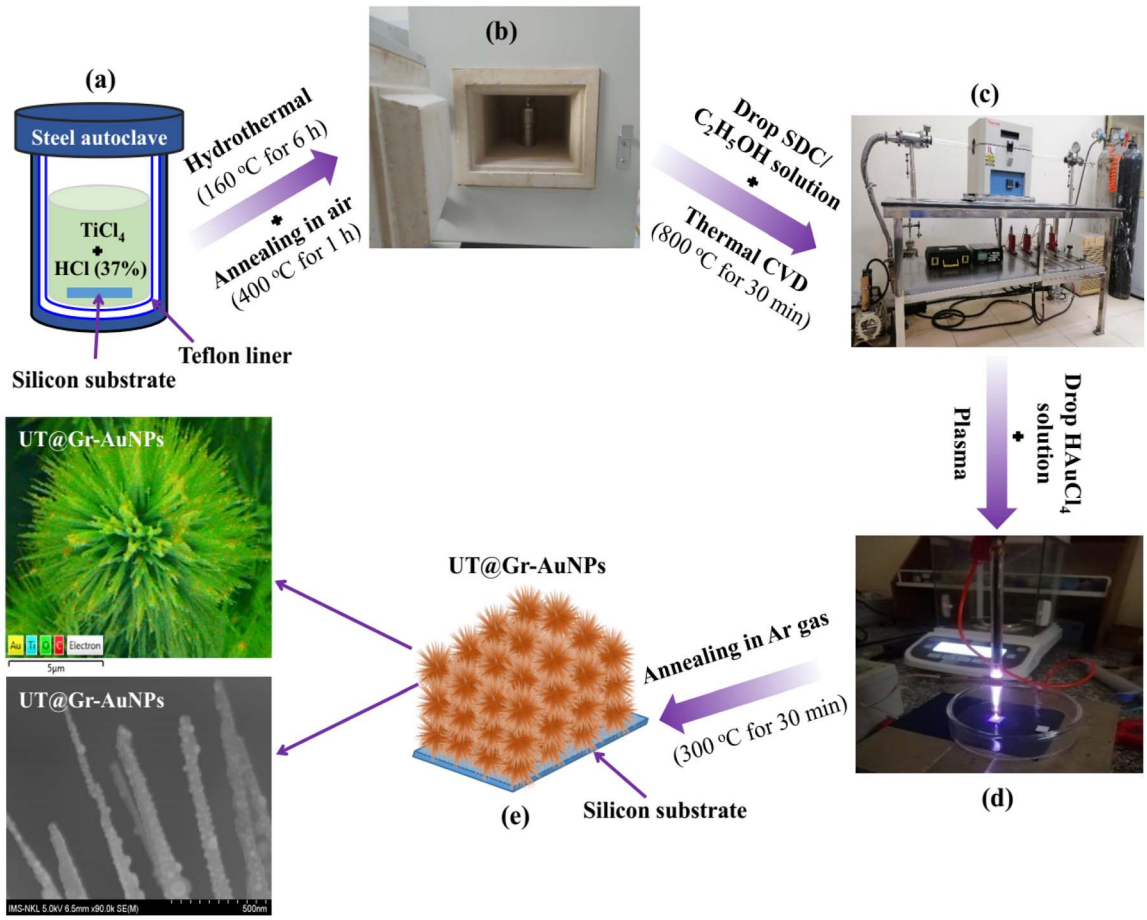


Scheme 1 Steps for fabrication of UT@Gr-AuNPs SERS substrates: (a) silicon substrates were placed in a steel autoclave containing a mixture solution of $TiCl_4$ and HCl (37%), (b) steel autoclave was kept at 160 °C for 6 h and annealed at 400 °C for 1 h in a muffle furnace, (c) thermal CVD process was performed at 800 °C for 30 min after the UT samples were coated by SDC/$C_2H_5OH$ solution, (d) plasma process was performed after the UT@Gr samples were coated by $HAuCl_4$ solution, and (e) UT@Gr-AuNPs samples were obtained after annealing at 300 °C for 30 min in Ar gas.

nanostructured noble metals such as Au and Ag can be considered as one of the promising materials for fabricating SERS substrates with good sensitivity and self-cleaning ability for photocatalytic decomposition of analyte molecules.[1,21,27]

In previous publications on graphene@$TiO_2$@noble metals nanocomposite for SERS and photocatalysis, graphene oxide (GO) nanosheets synthesized by the modified Hummers' method were usually combined with $TiO_2$ and noble metals nanoparticles.[2,21] $TiO_2$ and gold nanoparticles (AuNPs) were decorated onto the surface of reduced graphene oxide (rGO) *via* a two-step hydrothermal approach.[21] Recently, highly sensitive and good reusability SERS substrates based on silver nanoparticles (AgNPs) decorated $TiO_2$ with rGO nanosheets were also reported.[2,12,28] Apart from the rGO nanosheets, the graphene (Gr) films fabricated *via* the thermal chemical vapor deposition (CVD) method were combined with $TiO_2$ and noble metal nanoparticles.[1] Gr films fabricated after the CVD process were etched and transferred from the copper substrate to the AgNPs/$TiO_2$NPs SERS substrate.[1] However, $TiO_2$ materials used in previous graphene@$TiO_2$@noble metals composite SERS substrates have structures of zero-dimensional,[1] one-dimensional,[2] or two-dimensional,[28] which may limit the SERS signals and photocatalytic activity. Therefore, the development of novel methods for the fabrication of SERS substrates based on three-dimensional (3D) structure material of $TiO_2$@graphene with noble metals is still demanding and highly necessary.

In this work, 3D urchin-like titanium dioxide@graphene–gold nanoparticles (UT@Gr–AuNPs) architectures on silicon substrates were fabricated by growing of Gr shell layer on the UT core layer *via* thermal CVD technique using SDC as carbon source, followed by depositing AuNPs onto the UT@Gr *via* cold plasma (CP) process. The fabrication process of UT@Gr–AuNPs SERS substrates was depicted in Scheme 1. The SERS substrates based on UT@Gr–AuNPs architectures were used to detect and decompose rhodamine 6G (R6G) and rhodamine B (RhB) molecules at room temperature under ultraviolet light (UV, 254 nm) irradiation. These SERS substrates were also used to detect a pesticide, *e.g.*, malathion.

## 2. Experimental

### 2.1. Chemicals

Titanium tetrachloride ($TiCl_4$, 99%), gold(III) chloride trihydrate ($HAuCl_4 \cdot 3H_2O$, 99.99%), hydrochloric acid (HCl, 37%), absolute

ethanol ($C_2H_5OH$, 99.7%), rhodamine 6G (R6G, ≥99%), and rhodamine B (RhB, 99%) were obtained from Macklin Co., Ltd (China). Sodium deoxycholate (SDC, 96%) was obtained from Fujifilm Co., Ltd (Japan). Malathion was purchased from LGC (UK, 95%). Gases such as argon (Ar, >99%) and hydrogen ($H_2$, >99%) were obtained from Messer Co. Ltd. (Hai Phong, Vietnam). Silicon wafer (thick: 500 μm; Res.: ≤0.005 Ω) was purchased from Silicon Technology Corp. (Japan). Deionized (DI) water with a resistivity of 18.2 MΩ cm was utilized.

### 2.2. Preparation of UT@Gr–AuNPs

The synthesis process of UT@Gr–AuNPs SERS substrates was depicted in Scheme 1. Firstly, 0.3 mL $TiCl_4$ was added to a mixture of 8 mL HCl and 4 mL deionized (DI) water, stirred at 7–10 °C for 20 min. The mixture was then transformed into a Teflon-lined stainless steel autoclave, followed by placing the silicon substrates horizontally at the bottom of the autoclave (Scheme 1a). After that, the Teflon-lined stainless steel autoclave was kept at 160 °C for 6 h and then naturally cooled to room temperature (Scheme 1b). To obtain UT samples, the as-prepared samples were washed several times with ethanol and DI water to remove the other impurities and unreacted chemicals, then the samples were annealed at 400 °C for 1 h in a muffle furnace in air. For preparation of UT@Gr samples, an amount of 30 μL SDC/$C_2H_5OH$ mixture solution with a ratio of 3/1 was coated onto the surface of UT samples. The UT samples coated by SDC were then placed into the quartz tube for the thermal CVD process. The thermal CVD process was performed at 800 °C for 30 min in a gas mixture of Ar/$H_2$ (50/30 sccm) (Scheme 1c). After the thermal CVD process, the samples were cooled down to room temperature in Ar gas (50 sccm). For preparation of UT@Gr–AuNPs samples, 5 μL of 0.05 mM $HAuCl_4 \cdot 3H_2O$ solution was dropped onto the surface of UT@Gr substrates following by CP process for 3 min in a gas atmosphere of Ar (0.5 L $min^{-1}$), a current (3.5 mA), a DC voltage generator (11 V), and plasma power (0.2 W). The samples were placed under the CP source with a distance of 0.5 cm (Scheme 1d). After the CP process, the as-prepared samples were annealed at 300 °C for 30 min in Ar gas, and UT@Gr–AuNPs samples were obtained (Scheme 1e). The configuration of the CP system was presented by Xuan *et al.*[29]

### 2.3. Characterization

The surface morphology of the samples was examined by field emission scanning electron microscopy (FESEM, Hitachi S-4800) and transmission electron microscopy (TEM, JEM 2100, Jeol). The crystalline structure of the samples was analyzed by X-ray diffraction (XRD) recorded on a D8 Advance, Bruker. The presence of elements was confirmed by an energy dispersive X-ray spectroscopy (EDS) recorded on a SEM, JSM-IT800, Jeol. The adsorption of the samples was examined by UV-visible absorption spectrophotometer (UV-2450, UV/vis spectrophotometer, Shimadzu).

### 2.4. SERS activity measurements

SERS activity experiments of UT@Gr–AuNPs were evaluated by detecting the Raman signals of R6G and malathion molecules. 20 μL R6G solution ($10^{-2}$ M to $10^{-10}$ M) as well as 20 μL malathion solution with concentration ranging from $10^{-4}$ M to $10^{-7}$ M were directly deposited onto the surface of UT@Gr–AuNPs samples and dried at room temperature in an air atmosphere. The SERS performance for R6G and malathion on the UT@Gr–AuNPs samples was estimated *via* a Raman spectrophotometer recorded on a LabRAM HR Evolution, Horiba, with measurement parameters of excitation wavelength (532 nm), objective microscope (100×), laser power (100 mW), and laser spot (~1.0 μm). For analyzing the photocatalytic degradation activity of R6G molecules on UT@Gr–AuNPs SERS substrates, 20 μL R6G solution with $10^{-5}$ M concentration was directly deposited onto the surface of UT@Gr–AuNPs SERS substrates and dried in an air atmosphere. Then, these SERS samples were placed under an ultraviolet light (UV) lamp ($\lambda$ = 254 nm, 66 W) with a distance of 5 cm. The photocatalytic degradation activities were also estimated by a Raman spectrophotometer. The samples were withdrawn for analysis every 20 min under UV light illumination. All the measurements were repeated three times to evaluate the repeatability of the fabricated SERS substrates.

## 3. Results and discussions

### 3.1. Morphological and crystalline structure characterizations

The morphological characteristics of the UT, UT@Gr and UT@Gr–AuNPs samples were determined by SEM, as shown in Fig. 1. It is observed that UT has a 3D urchin structure with the length of UT rods of ~5 μm (Fig. 1a). The UT structure remains after the CVD process for the synthesis of the Gr shell layer (Fig. 1b). Fig. 1c and d are the SEM images of the UT@Gr–AuNPs sample with low magnification and high magnification, respectively. It can be observed that after the CP process, AuNPs with a diameter of ~10–50 nm are uniformly deposited on the side and top of the UT nanoneedles. Fig. 1e and f show the typical TEM images of the UT@Gr–AuNPs nanoneedles with low magnification and high magnification, respectively. Fig. 1f indicates that the distance between the lattice of the UT crystal is 0.32 nm and the thickness of the Gr shell is about 10 nm.

The homogeneous distribution of Ti, O, C, and Au elements on the surface of UT@Gr–AuNPs sample was determined *via* SEM-EDS mapping, as shown in Fig. 2. The EDS results show the distribution of Ti (cyan), O (green), C (red) and Au (yellow) elements, and the corresponding contents are 49.3, 39.2, 3.4, and 8.1 wt%, respectively. The SEM-EDS mapping results show that the UT nanoneedles core is fully surrounded by the carbon (C) shell; in addition, AuNPs are also anchored onto the surface of the UT@Gr nanoneedles.

The crystal structure of the UT@Gr and UT@Gr–AuNPs samples was determined by XRD, as shown in Fig. 3. As presented in Fig. 3a, all the main diffraction peaks of rutile $TiO_2$ for all the three samples are observed at $2\theta$ = 27.5°, 36.1°, 39.2°, 41.3°, 44.1°, 54.4°, 56.7°, 62.8°, and 64.1° corresponding to the crystal facets (110), (101), (200), (111), (210), (211), (220), (002), and (310), respectively.[30] These diffraction peaks are shaped and intense with the standard $TiO_2$ (PDF no. 01-087-0710). These

 

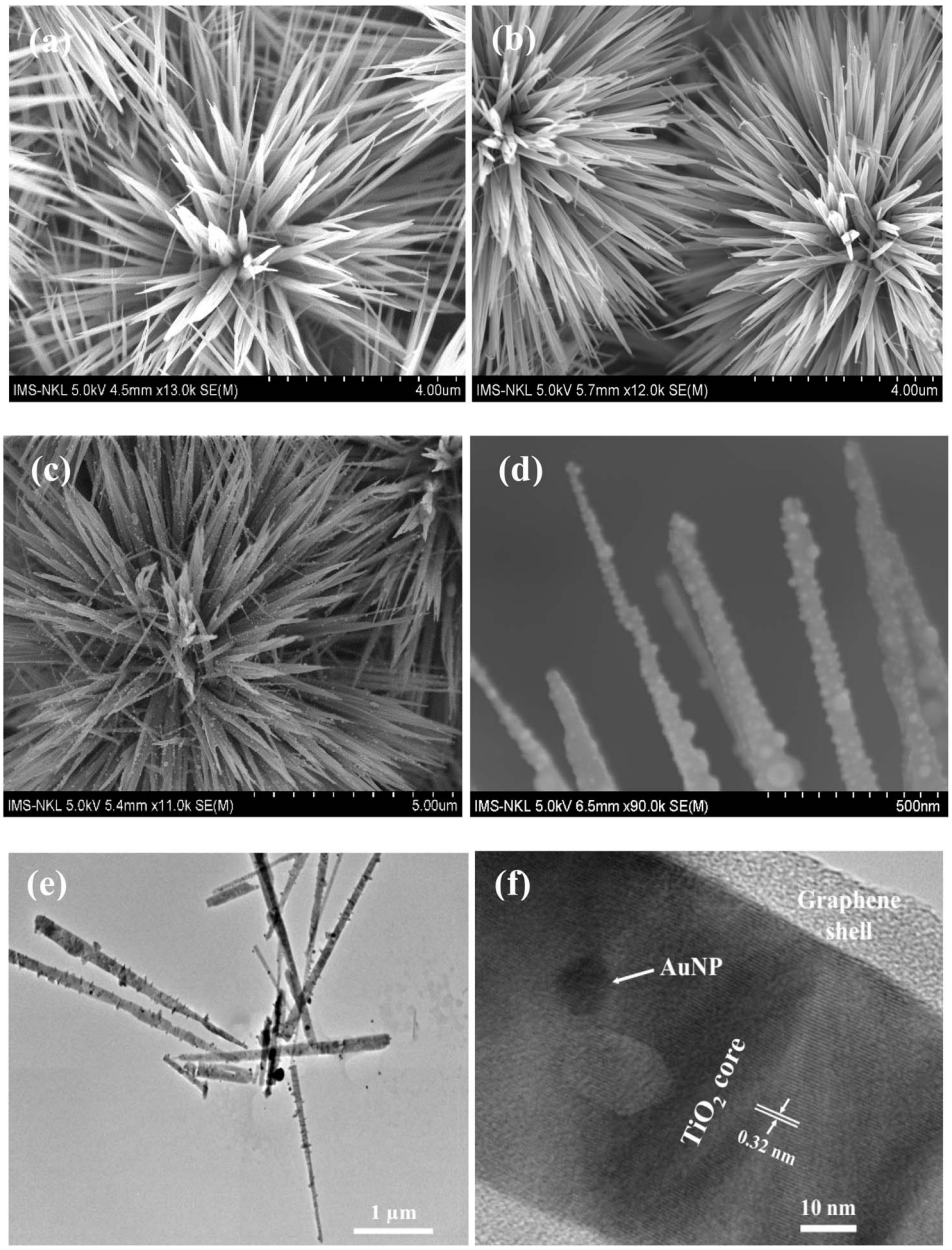


Fig. 1 SEM images of (a) UT, (b) UT@Gr, (c and d) UT@Gr–AuNPs. Typical TEM images (e and f) of UT@Gr–AuNPs.

results show that the crystallinity of UT nanoneedles of UT@Gr and UT@Gr–AuNPs samples is the same. After the modification process, the diffraction peaks of Au nanocrystalline in the XRD pattern of UT@Gr–AuNPs (Fig. 3b) can be seen at $2\theta = 38.1°$, 44.3°, and 64.1°, and they are indexed to the (111), (200), and (220) planes (PDF no. 01-073-9564), respectively. The above characterization results confirm that the UT core is completely covered by the Gr shell *via* thermal CVD process with SDC as carbon source. The AuNPs were directly synthesized onto the surface of UT@Gr samples *via* the CP method. The mechanism for the formation of the Gr shell on the surface of UT nanoneedles can be explained as that: at a high temperature of 800 °C, SDC decomposed into carbon atoms, and these carbon atoms precipitated onto the surface of UT nanoneedles to form a Gr shell. The mechanism for the formation of UT structure may follow a process of nucleation, dissolution, recrystallization, and self-assembly of the UT nanoneedles.[31] The mechanism for the formation of the AuNPs onto the surface of UT@Gr samples *via* the reduction of gold ions by pure argon plasma jet is described below. The reduction of gold ion ($Au^{3+}$) from $HAuCl_4$ solution to form zero-valent gold ($Au^0$) nanoparticles can be described in three pathways ((a), (b), and (c)):[29,32]

(a) Electrons generated from plasma can be solvated in $H_2O$ and directly used for the reduction of $Au^{3+}$ ions to form Au seeds that grow into AuNPs.

$$Au^{3+} + 3e^- \rightarrow Au^0 \quad (1)$$

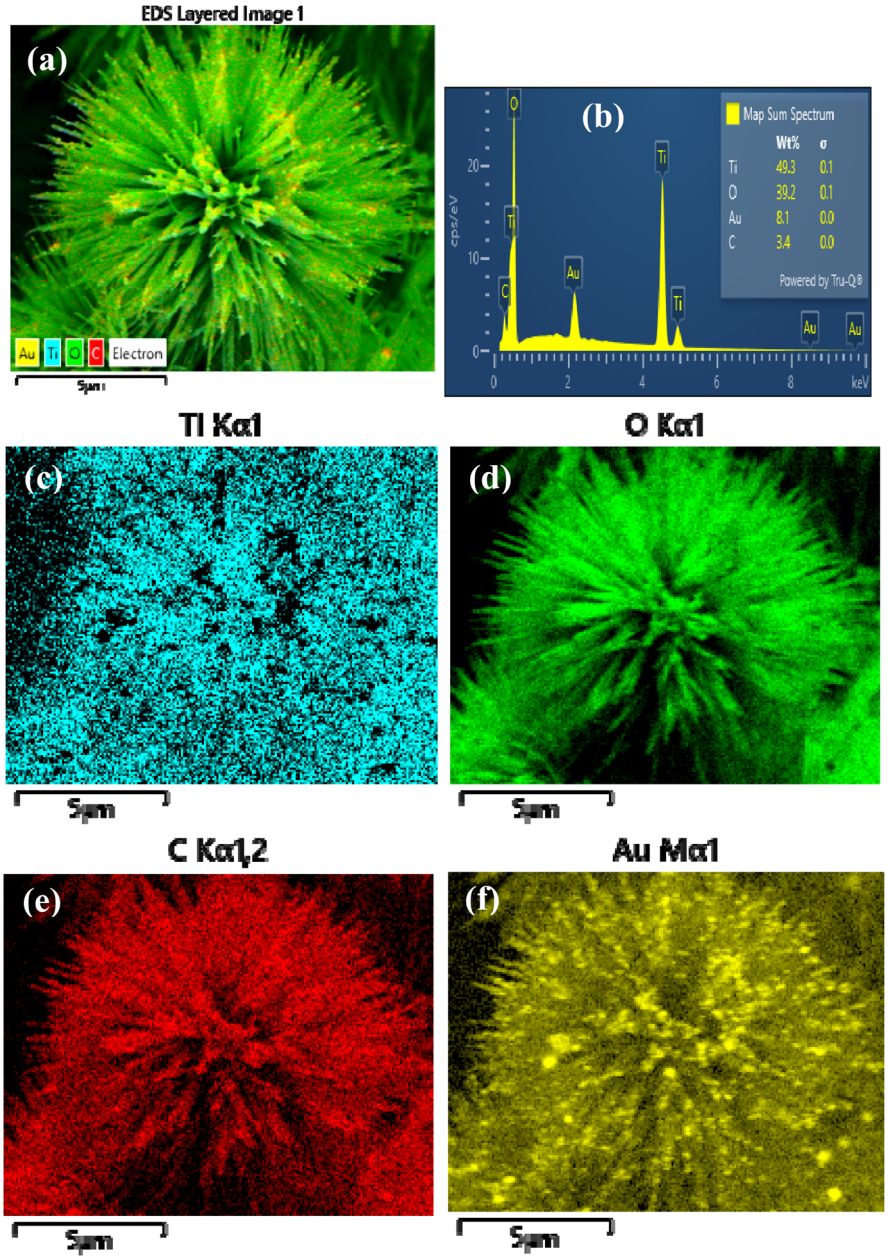


Fig. 2 (a) SEM image, (b) EDS spectrum, (c–f) mapping images of elements for (c) Ti; (d) O; (e) C; (f) Au of UT@Gr–AuNPs.

(b) Plasma electrons can react with $H_2O$ molecules on the surface of UT@Gr to form hydroxyl radicals ($OH^{\bullet}$). These $OH^{\bullet}$ radicals can quickly react to form $H_2O_2$. This $H_2O_2$ can reduce $Au^{3+}$ ions to form Au seeds that grow into AuNPs, as illustrated by the following:

$$e_{plasma}^{-} + H_2O \rightarrow OH^{\bullet} + H^{-} \quad (2)$$

$$2OH^{\bullet} \rightarrow H_2O_2 \quad (3)$$

$$3H_2O_2 + 3OH^{-} + Au^{3+} \rightarrow Au^{0} + 3HO_2 + H_2O \quad (4)$$

(c) Electron–hole pairs generated from plasma under UV light can be used to directly reduce $Au^{3+}$ ions on the surface of UT@Gr nanoneedles or to generate radicals that can subsequently be used to reduce $Au^{3+}$ ions.

Raman spectra were recorded to estimate the structure of UT@Gr and UT@Gr–AuNPs samples. As shown in Fig. 4, Raman spectra of all the samples show three characteristic peaks of $TiO_2$ at 231, 443, and 608 $cm^{-1}$, and three characteristic peaks of Gr at 1343, 1578, and 2700 $cm^{-1}$. The peaks at 231, 443, and 608 $cm^{-1}$ are assigned to the $TiO_2$ rutile phase.[33] The peak at 1343 $cm^{-1}$ (D band) is assigned to the presence of structural disorder and defects in the Gr structure.[33,34] The peak at 1578 $cm^{-1}$ (G band) is ascribed to the stretching of the carbon–carbon bonds in the $sp^2$ system of Gr structure.[34–36] The peak at 2700 $cm^{-1}$ (2D band) is related to the second harmonic of the D

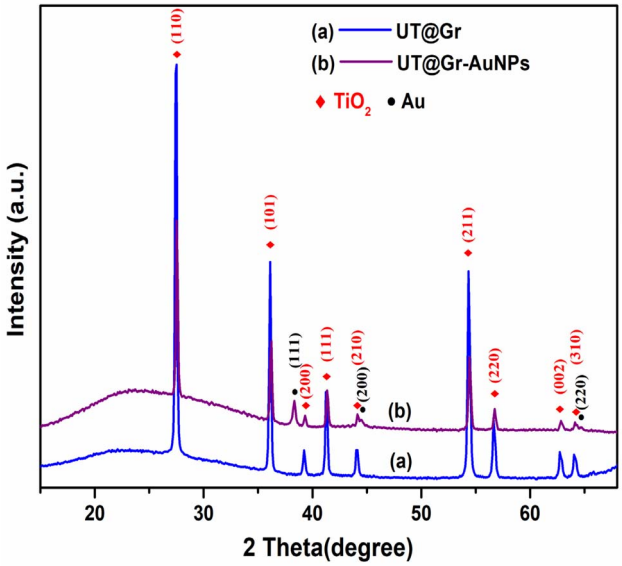


Fig. 3 XRD spectra of (a) UT@Gr and (b) UT@Gr–AuNPs samples.

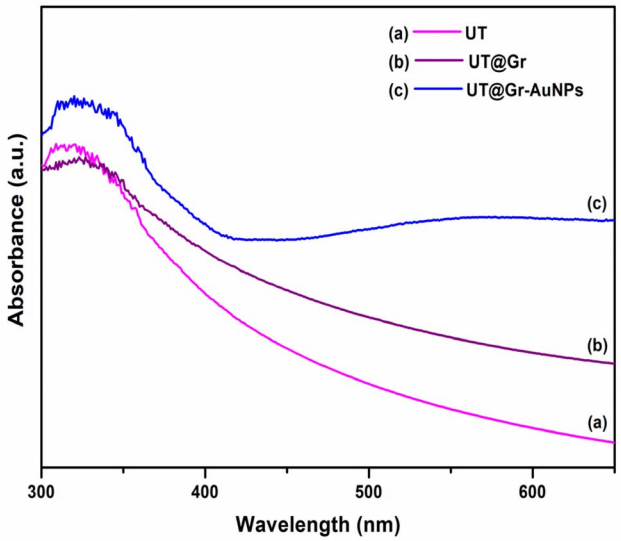


Fig. 5 UV-vis spectra of (a) UT, (b) UT@Gr and (c) UT@Gr–AuNPs samples.

band.[36] After UT@Gr was modified, all the Raman peak positions of $TiO_2$ and Gr are no change as compared with those of the UT@Gr sample. However, the $I_D/I_G$ intensity ratio for UT@Gr was found to be 0.79, and this ratio was lower than for UT@Gr–AuNPs (0.91). The increase of the $I_D/I_G$ ratio signals for UT@Gr–AuNPs is ascribed to the increase in some lattice defects due to the chemical interaction between AuNPs and Gr.[37]

### 3.2. Optical characterizations

Fig. 5a–c present UV-vis absorption spectra of UT, UT@Gr and UT@Gr–AuNPs samples, respectively. The absorption edge of UT was found to be ~380 nm. Compared to UT, the absorption edge of UT@Gr shifts toward visible region due to strong interaction between Gr and UT.[38] Compared to UT and UT@Gr, UT@Gr–AuNPs shows a broad absorption band (~500–600 nm) in the visible region. This can be ascribed to the localized surface plasmon resonance (LSPR) absorption of AuNPs.[38,39] It is clearly that after addition of Gr and Au, the visible light absorption is increased.

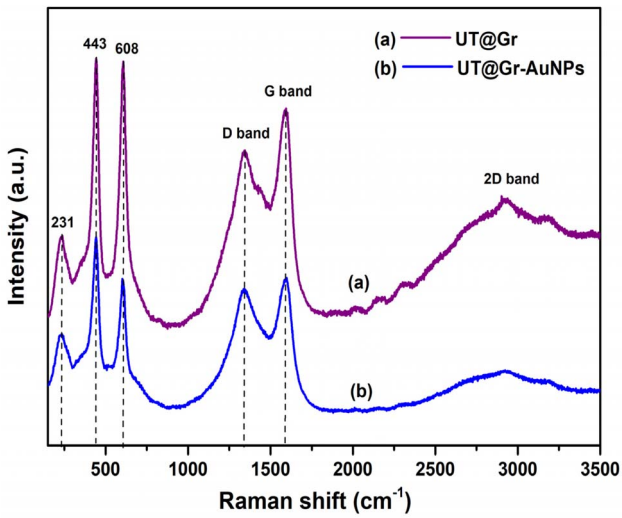


Fig. 4 Raman spectra of (a) UT@Gr and (b) UT@Gr–AuNPs samples.

### 3.3. SERS characteristics

Fig. 6 presents Raman spectra of R6G with a concentration of $10^{-2}$ M on $Si/SiO_2$ substrate (Fig. 6a) and of R6G with a concentration of $10^{-5}$ M on UT (Fig. 6b), UT@Gr (Fig. 6c), and UT@Gr–AuNPs (Fig. 6d) samples. As presented in Fig. 6a and b, when $Si/SiO_2$ substrate and UT are used as SERS substrates, Raman scattering signals of R6G molecules are not detected. As presented in Fig. 6c, the Raman spectrum of UT@Gr shows strong signals of R6G molecules at 611, 771, 1187, 1360, 1506, 1538, 1569, and 1649 $cm^{-1}$.[1,40] The peaks at 611, 771, and 1187 $cm^{-1}$ are assigned to the vibration modes of the C–C–C in-plane bend, C–H out-of-plane bend, and C–H in-plane bend, respectively.[41] The peaks at 1360, 1506, 1538, and 1649 $cm^{-1}$ can be attributed to the vibration modes of the aromatic C–C stretching.[41,42] The peak at 1569 $cm^{-1}$ is assigned to the N–H in-plane bend modes.[43] Compared to the UT substrate without the Gr shell, the intensity enhancement of R6G Raman signals on UT@Gr substrate (Fig. 6d) can be explained as follows: the excited electrons of UT can be transferred into Gr from the surface stage energy levels of UT. The Gr shell acts as the electron acceptor of UT and prevents the recombination of charge, and provides an indirect charge transfer from UT to R6G molecules. On the other hand, with good conductivity, the Gr can promote the transport of charge carriers from UT to R6G molecules. Therefore, a rapid interfacial charge transfer between UT and Gr would enhance the SERS signals of the R6G molecules.[44] More interestingly, when UT@Gr–AuNPs are used as SERS substrates, the intensity of these Raman signals of R6G molecules is significantly enhanced by about 6.3 times

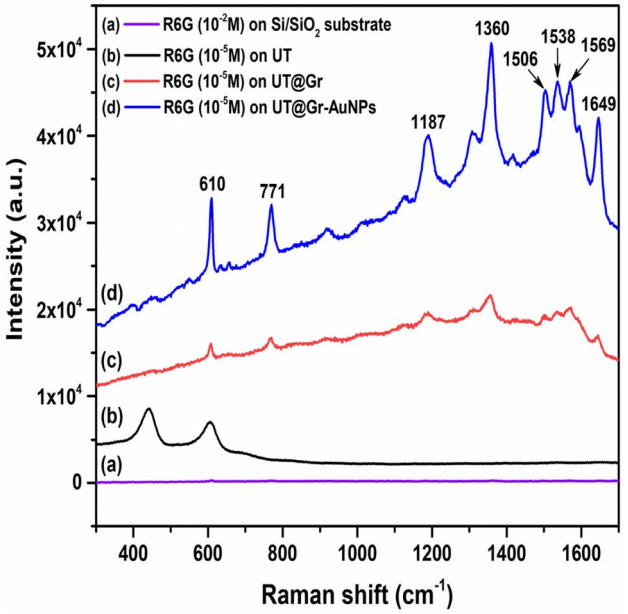


Fig. 6 SERS spectra of R6G adsorbed on: (a) a Si/SiO$_2$ sample with the concentration of $10^{-2}$ M, (b) UT, (c) UT@Gr, and (d)UT@Gr–AuNPs samples with the concentration of $10^{-5}$ M.

compared with the UT@Gr substrate without AuNPs. This enhancement can be explained due to the EM enhancement caused by the surface plasmon resonance (SPR) of the AuNPs. Fig. 7a shows the Raman spectra of R6G with concentrations of $10^{-5}$ M to $10^{-10}$ M adsorbed on UT@Gr–AuNPs SERS substrate. Raman signals were collected from the baseline and averaged from three repetitions. The concentration dependence was determined by measurement from seven randomly distributed locations for each concentration of R6G in an area of 10 × 10 μm$^2$ on the surface of UT@Gr–AuNPs SERS substrates. It can be seen that the Raman intensities of R6G increase with the successive increase in concentration of the probe molecule, as shown in Fig. 7b.

The enhancement factor (EF) of the SERS substrates can be estimated *via* the equation:[45,46]

$$\mathrm{EF} = (I_{\mathrm{SERS}}/I_{\mathrm{Ref}}) \times (C_{\mathrm{Ref}}/C_{\mathrm{SERS}}) \quad (5)$$

where $I_{\mathrm{SERS}}$ and $I_{\mathrm{Ref}}$ are the Raman intensities of R6G adsorbed on SERS substrate and Si/SiO$_2$ non-SERS substrate, respectively. $C_{\mathrm{SERS}}$ and $C_{\mathrm{Ref}}$ are the corresponding concentrations of R6G dropped on SERS substrate ($10^{-5}$ M) and Si/SiO$_2$ substrate ($10^{-2}$ M), respectively.

The limit of detection (LOD) of the SERS substrates can be estimated *via* the equation:[47]

$$\mathrm{LOD} = 3 \times S_{\mathrm{w}}/b \quad (6)$$

where $S_{\mathrm{w}}$ denotes the standard deviation of the blank sample (water), $b$ shows the slope of the calibration curve. At the peak of 771 cm$^{-1}$, the EF using eqn (5) obtained as 1.3 × 10$^6$ (UT@Gr) and 8.6 × 10$^6$ (UT@Gr–AuNPs), and the LOD using eqn (6) obtained as 6.38 × $10^{-10}$ M (UT@Gr) and 5.86 × $10^{-11}$ M

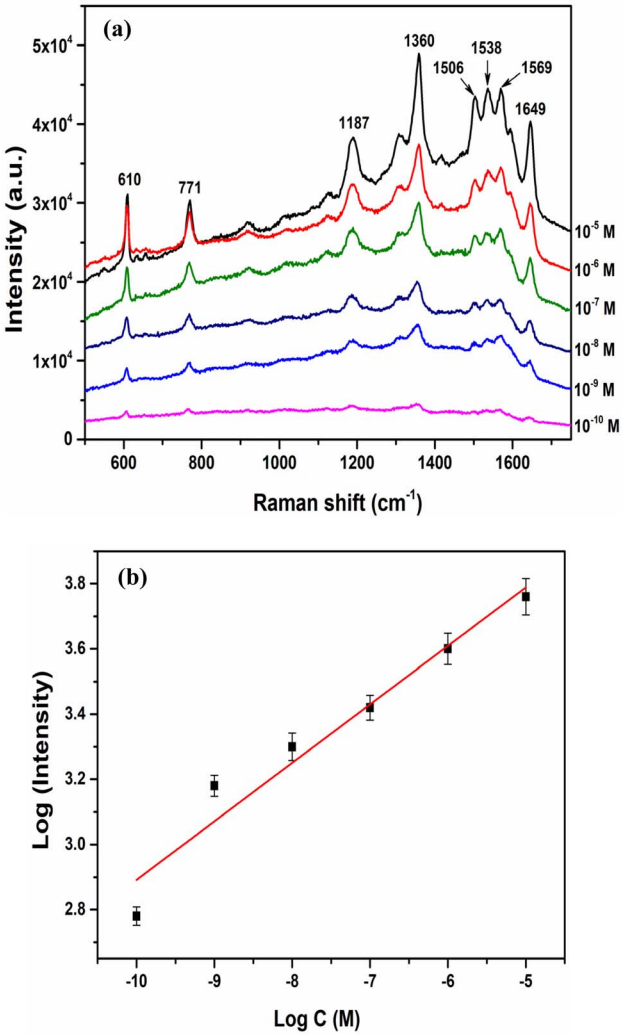


Fig. 7 (a) SERS spectra of R6G molecules with the concentrations of $10^{-5}$ M to $10^{-10}$ M adsorbed on UT@Gr–AuNPs samples and (b) the change of peak intensity at 771 cm$^{-1}$ as a function of concentration.

(UT@Gr–AuNPs). Furthermore, the repeatability of SERS substrates was also investigated. Fig. 8a and b present the Raman spectra of $10^{-5}$ M R6G adsorbed on the surface of UT@Gr–AuNPs for two different batches with five random measurement points. The relative standard deviations (RSD) of the SERS intensity at 771 cm$^{-1}$ and 1649 cm$^{-1}$ were found to be 14.8% (Fig. 8c), and 13.1% (Fig. 8e) for batch 1 and 13.9% (Fig. 8d), and 12.8% (Fig. 8f) for batch 2, respectively. The proposed UT@Gr–AuNPs SERS substrate could be used for quantitative detection because the RSD values of this material were lower than 20%.[5,6,48,49] In addition to evaluating the SERS ability to detect the R6G molecules, the UT@Gr–AuNPs SERS substrates were also used for detecting the concentration of malathion pesticide residue.

### 3.4. The photocatalytic activity of R6G molecules on UT@Gr–AuNPs SERS substrate

Fig. 9a shows the Raman spectra of $10^{-5}$ M R6G on UT@Gr–AuNPs SERS substrate with UV irradiation times ranging from

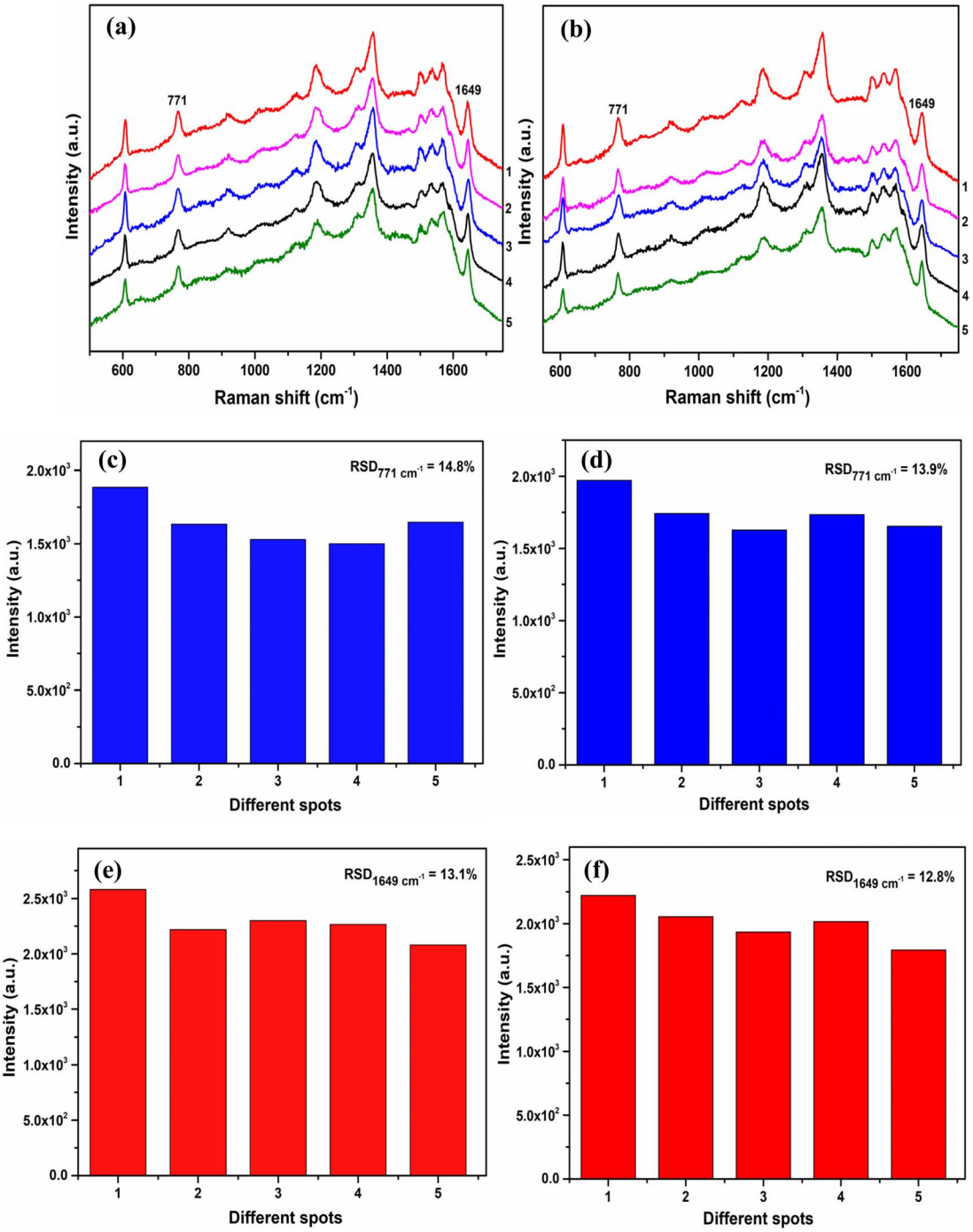


Fig. 8 SERS spectra of $10^{-5}$ M R6G molecules adsorbed on the surface of UT@Gr–AuNPs for two different batches: (a) batch 1, and (b) batch 2. The RSD values at peaks: 771 $cm^{-1}$ for (c) batch 1 and (d) batch 2; 1649 $cm^{-1}$ for (e) batch 1 and (f) batch 2.

0 to 80 min. As shown in Fig. 9a, the Raman signals of R6G gradually disappear with increasing UV irradiation time. The photocatalytic efficiency of UT@Gr–AuNPs SERS substrate can be characterized *via* the R6G Raman peak intensity at 771 $cm^{-1}$. The photocatalytic rate ($k$) of R6G is estimated by $\ln(I/I_0)$ *versus* the irradiation time (Fig. 9b), where $I$ and $I_0$ are related to the Raman peaks intensity of R6G molecules after different UV irradiation times and after initial adsorption–desorption equilibrium. Based on the slope of the fitting curve in Fig. 9b, $k$ was estimated to be 0.035 $min^{-1}$. Compared with previously presented SERS substrates, the UT@Gr–AuNPs SERS substrate demonstrated efficient R6G degradation under UV irradiation (254 nm) (Table 1).

The charge transfer and photocatalytic mechanism of the UT@Gr–AuNPs material towards R6G are shown in Fig. 10. Under the adsorption light photons of UV lamp source, the

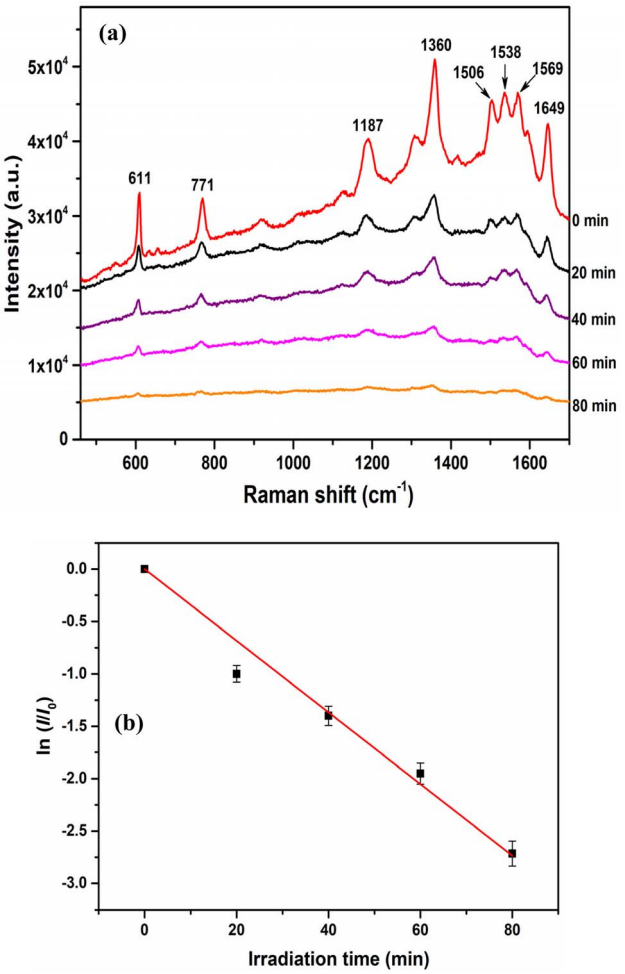


Fig. 9 (a) SERS spectra and (b) linear relationship between the irradiation time and the logarithm of SERS intensities at 771 $cm^{-1}$ for the degradation of R6G molecules.

electrons from the surface of UT are excited to produce electron–hole pairs ($e^-$ and $h^+$), and the AuNPs deposited on the surface of the UT@Gr could be excited to produce hot $e^-$–$h^+$ pairs. Under the surface plasmon resonance of AuNPs, the separation of photogenerated $e^-$–$h^+$ pairs could be enhanced.[57] The photo-generated $e^-$ in the conductive band of UT can quickly transfer to Gr as well as AuNPs and react with dissolved oxygen ($O_2$) molecules of R6G solution to form radical anions $*O_2^-$. On the other hand, the photo-generated holes can be accepted by AuNPs to obtain the separation $e^-$/$h^+$ pairs and react with $H_2O$ to produce reactive hydroxyl radicals *OH. These produced radical anions $*O_2^-$ combine with $H_2O$ to form *OH radicals, which degrade R6G molecules to $CO_2$ and $H_2O$.[21,58] The reaction equations involved in the photocatalytic mechanism are shown by eqn (7)–(15).[58,59]

$$UT + h\nu \rightarrow UT\,(h^+ + e^-) \quad (7)$$

$$UT\,(h^+ + e^-) + Gr \rightarrow Gr\,(e^-) + UT\,(h^+) \quad (8)$$

$$Gr\,(e^-) + Au \rightarrow Au\,(e^-) + Gr \quad (9)$$

Table 1 Comparison of photocatalytic activity towards R6G molecules degradation from different SERS substrates[a]

| SERS substrate for photocatalytic degradation | Irradiation source | Complete degradation time (min) | Concentration (mol $L^{-1}$) | Degradation rate ($k$) $min^{-1}$ | Ref. |
|---|---|---|---|---|---|
| g-$C_3N_4$/AuNPs | Xenon lamp ($\lambda$ < 420 nm) | 20 | $10^{-5}$ | 0.1102 | 50 |
| $TiO_2$/Au nanowire arrays | Xenon lamp ($\lambda$ < 420 nm) | 120 | $10^{-4}$ | NA | 40 |
| $TiO_2$–Au–rGO | Xenon lamp ($\lambda$ > 400 nm) | 80 | $10^{-4}$ | 0.03785 | 21 |
| Au–ZnO@NWFs | Mercury lamp | 15 | $10^{-6}$ | NA | 51 |
| Au/graphene/Ag@ZnO | Xenon lamp | 120 | $10^{-6}$ | NA | 52 |
| Ag–G–$TiO_2$/G–Ag–$TiO_2$/Ag–$TiO_2$–G | UV | 60 | $10^{-6}$ | 0.0371/0.0301/0.0111 | 12 |
| $TiO_2$–AgNPs | UV ($\lambda$ = 385 nm) | 120 | $10^{-6}$ | 0.029 | 22 |
| Ag–$TiO_2$ nanotube arrays | UV ($\lambda$ = 365 nm) | 150 | $10^{-7}$ | NA | 53 |
| $TiO_2$/Ag/NF | UV ($\lambda$ = 365 nm) | 180 | $10^{-6}$ | NA | 23 |
| Ag–$TiO_2$ nanorods | UV ($\lambda$ = 254 nm) | 90 | $10^{-5}$ | 0.043 | 54 |
| Ag/$TiO_2$ NTs | UV ($\lambda$ = 254 nm) | 140 | $10^{-6}$ | 0.02479 | 55 |
| Ag/GO/TNR | Xenon lamp | 60 | $10^{-6}$ | NA | 56 |
| UT@Gr–AuNPs | UV ($\lambda$ = 254 nm) | 80 | $10^{-5}$ | 0.035 | This work |

[a] NWFs, nano forests; NF, nickel foam; TNR, $TiO_2$ nanorod array.

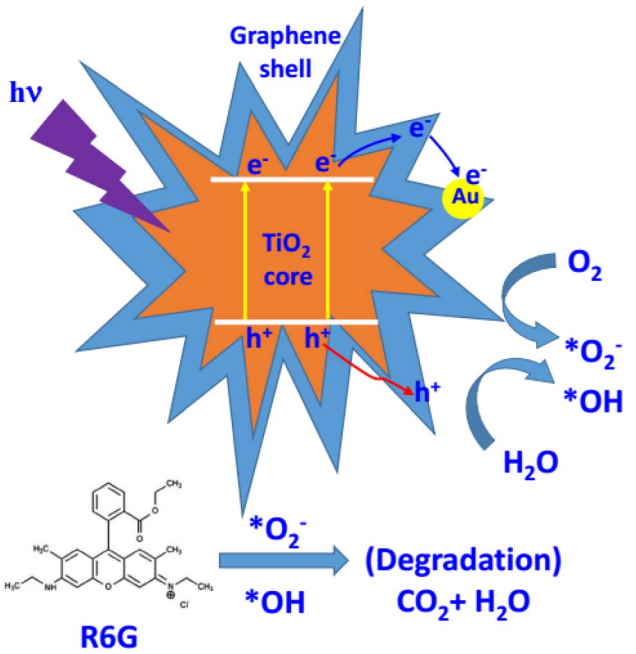


Fig. 10 Illustration of charge transfer in UT@Gr–AuNPs and the proposed photocatalytic degradation mechanism of R6G molecules.

$$Au/Gr\ (e^-) + O_2 \rightarrow Au/Gr + {}^*O_2^- \quad (10)$$

$${}^*O_2^- + H_2O \rightarrow HO_2^* + OH^- \quad (11)$$

$$HO_2^* + H_2O \rightarrow H_2O_2 + {}^*OH \quad (12)$$

$$H_2O_2 \rightarrow 2{}^*OH \quad (13)$$

$$h^+ + OH^- \rightarrow {}^*OH \quad (14)$$

$$R6G + {}^*O_2^- + {}^*OH \rightarrow CO_2 + H_2O + \text{intermediates} \quad (15)$$

### 3.5. The recyclability of UT@Gr–AuNPs SERS substrates

The recyclability of UT@Gr–AuNPs SERS substrates was evaluated through three cycles for the detection of R6G and RhB molecules under UV (254 nm) light irradiation for 80 min. Fig. 11a and b show the SERS spectra of $10^{-5}$ M R6G and $10^{-5}$ M RhB molecules on the UT@Gr–AuNPs SERS substrates before and after self-cleaning for three cycles, respectively. It can be seen that the SERS peak intensities of both R6G and RhB molecules almost decay completely under UV light irradiation time of 80 min and can be restored after each cleaning and adsorption of R6G and RhB molecules. This indicated that the SERS substrates based on UT@Gr–AuNPs exhibit good self-cleaning under UV light irradiation and highly recyclable SERS activity for the detection of R6G and RhB molecules.

### 3.6. Detection of malathion pesticide

Fig. 12a shows the SERS spectra of malathion with the concentration from $10^{-4}$ M to $10^{-7}$ M. The SERS spectra of these

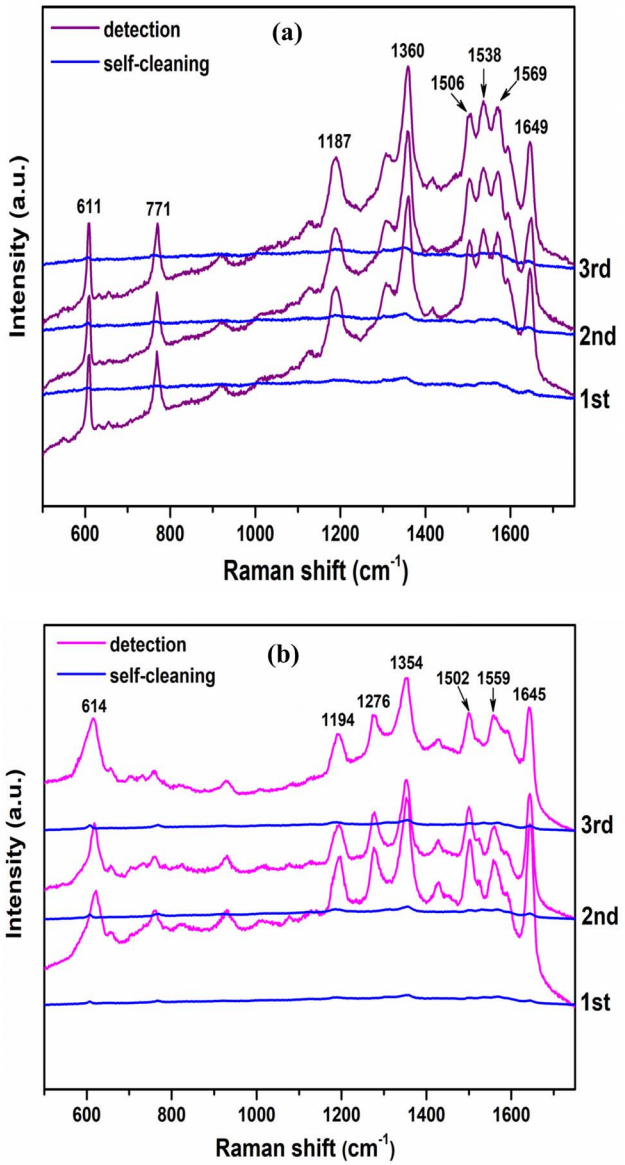


Fig. 11 SERS spectra of: (a) R6G ($10^{-5}$ M) and (b) RhB ($10^{-5}$ M) on the UT@Gr–AuNPs before and after self-cleaning for three cycles.

samples exhibit some strong vibrational signatures at 724, 1024, 1318, and 1528 $cm^{-1}$ corresponding to characteristic peaks of malathion molecules.[60–62] The Raman signal at these peaks gradually increases with increasing malathion concentration. The signal intensity increases with increasing malathion concentration can be explained due to the fact that at high concentrations, the malathion molecules are "crowded" and adsorbed on the substrate surface. The researchers observed that sulfur atoms of the malathion molecule with a P═S bond have a strong affinity for Au atoms. This makes the sulfur atoms of the malathion molecule to significantly participate in the adsorption process with the SERS substrate surface.[63,64] The characteristic peak at 724 $cm^{-1}$ corresponded to the stretchings of $\nu$(P═S); $\nu$(P–O) was selected to prove the presence of malathion.[60] Fig. 12b shows the plot of log(Raman intensity) of the

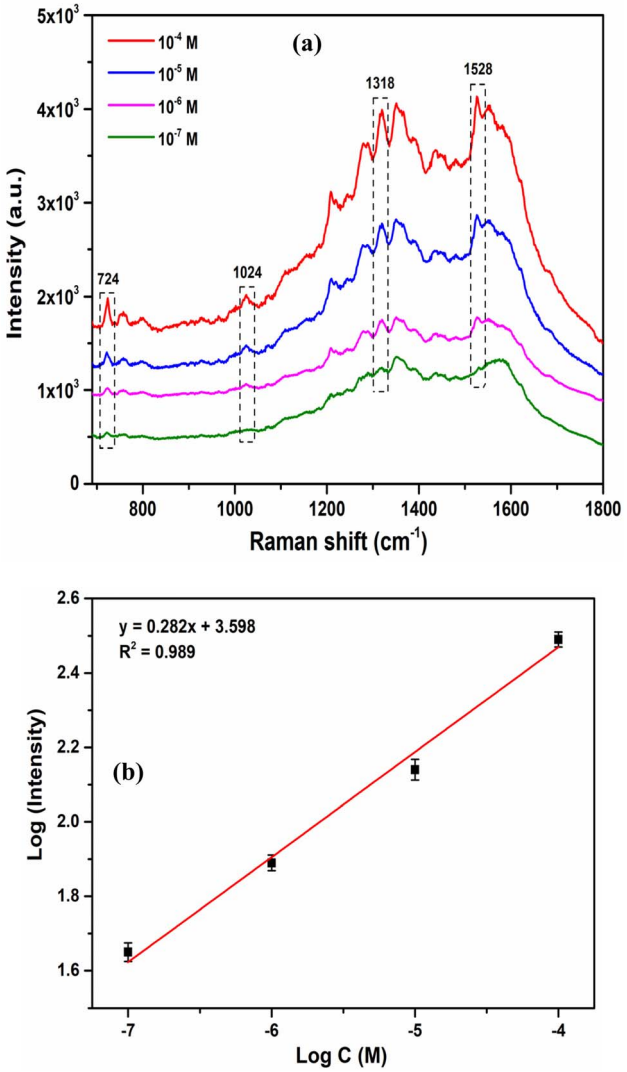


Fig. 12 (a) SERS spectra of different concentrations of malathion and (b) the change of peak intensity at 724 $cm^{-1}$ as a function of concentration.

characteristic peak at 724 $cm^{-1}$ *versus* log(concentration) of malathion. Using eqn (6), the LOD for detection of malathion was determined to be about $2.87 \times 10^{-8}$ M in a nearly linear relationship with $R^2 = 0.988$. This LOD value is lower than the maximum contaminant level of malathion in drinking water set by the United States Environmental Protection Agency (100 μg $L^{-1}$ ($3.027 \times 10^{-7}$ M) for children and 200 μg $L^{-1}$ ($6.054 \times 10^{-7}$ M) for adults)[65] and the European Union (20 μg $L^{-1}$ ($6.054 \times 10^{-8}$ M)).[66]

## 4. Conclusions

In this work, 3D urchin-like $TiO_2$@Gr–AuNPs (UT@Gr–AuNPs) architectures with a core@shell structure of UT@Gr decorated by AuNPs were successfully synthesized on silicon substrates. The Gr shell layer formed on the UT core layer was synthesized *via* thermal CVD technique using SDC as carbon source. The AuNPs were decorated onto the surface of UT@Gr *via* the cold plasma (CP) process. The UT@Gr–AuNPs were used as SERS substrates for the detection of R6G and malathion. The LODs of R6G and malathion were determined as $5.86 \times 10^{-11}$ M and $2.87 \times 10^{-8}$ M, respectively. Moreover, these SERS substrates prepared in this study effectively enable *in situ* SERS monitoring of the R6G and RhB photodegradation reaction and self-cleaning performance under ultraviolet light (UV, 254 nm) irradiation.

## Data availability

The datasets used and/or analyzed during the current study are available from the corresponding author upon reasonable request. In addition, all the data generated or analyzed during this study are included in this article.

## Author contributions

Nguyen Thi Huyen: methodology, investigation, formal analysis, data curation, conceptualization, data curation. Le Thi Quynh Xuan: investigation, formal analysis. Tran Ai Suong Suong: investigation, formal analysis. Cao Thi Thanh: investigation, formal analysis. Pham Van Trinh: investigation, formal analysis. Nguyen Van Tu: investigation, formal analysis. Nguyen Thu Loan: investigation. Luong Truc Quynh Ngan: investigation. Pham Thanh Binh: investigation. Cao Thi Linh Huong: investigation. Dao Nguyen Thuan: investigation. Vu Xuan Hoa: investigation. Nguyen Van Hao: investigation. Nguyen Van Quynh: investigation. Hiroya Abe: supervision, investigation. Nguyen Van Chuc: supervision, conceptualization, methodology, formal analysis, project administration, writing-original draft preparation, validation writing, reviewing, and editing. All authors discussed and approved the paper.

## Conflicts of interest

There are no conflicts to declare.

## Acknowledgements

This research is funded by the Vietnam National Foundation for Science and Technology Development (NAFOSTED) under grant number 103.99-2021.18.

## References

1 Z. Wang, S. Li, J. Wang, Y. Shao and L. Mei, *New J. Chem.*, 2022, **46**, 18787.
2 P. Butmee, A. Samphao and G. Tumcharern, *J. Hazard. Mater.*, 2022, **437**, 129344.
3 A. Jinachandran, T. Kokulnatan, T. J. Wang, K. M. A. Kumar, J. Kumar and R. Panneerselvam, *Microchim. Acta*, 2024, **191**, 347.
4 X. Wen, Y. Liu, W. Zhang, L. You, N. Cai and J. Li, *Food Chem.*, 2025, **464**, 141935.

5 K. Luo, A. Chen, Y. Liu, J. Yang, N. Cai and J. Li, *Ind. Crops Prod.*, 2025, **225**, 120453.
6 X. Wen, H. Cheng, W. Zhang, L. You and J. Li, *Talanta*, 2024, **266**, 125140.
7 N. S. Aminah, T. Lertvanithphol, A. Sathukarn, M. Horprathum, H. Alatas, V. Fauzia, S. P. Santosa, Isnaeni, Herman, A. Alni and M. Djamal, *Opt. Mater.*, 2024, **149**, 114952.
8 N. E. Markina, S. N. Ustinov, A. M. Zakharevich and A. V. Markin, *Anal. Chim. Acta*, 2020, **1138**, 9–17.
9 S. Lee, H. Cho, J. W. Hong and Y. W. Lee, *Mater. Lett.*, 2021, **284**, 128988.
10 R. Madhu, A. Karmakar, K. Karthick, S. Kumaravel, S. S. Sankar, D. Prajapati and S. Kundu, *Dalton Trans.*, 2021, **50**, 7198–7211.
11 A. Karmakar, K. Karthick, S. S. Sankar, S. Kumaravel and S. Kundu, *Appl. Surf. Sci.*, 2020, **527**, 146777.
12 X. Zhang, N. Wang, R. Liu, X. Wang, Y. Zhu and J. Zhang, *Opt. Mater. Express*, 2018, **8**, 704–717.
13 E. Rosqvist, U. Böcker, T. G. Sarfraz, N. K. Afseth, S. Tolvanen, J. Peltonen and J. Sarfraz, *Nano-Struct. Nano-Objects*, 2023, **34**, 100956.
14 T. T. H. Pham, X. H. Vu, N. D. Dien, T. T. Trang, N. V. Truong, T. D. Thanh, P. M. Tan and N. X. Ca, *RSC Adv.*, 2020, **10**, 24577–24594.
15 M. C. Nguyen, T. Q. N. Luong, T. T. Vu, C. T. Anh and T. C. Dao, *RSC Adv.*, 2022, **12**, 11583–11590.
16 S. Rani and A. K. Shukla, *Plasmonics*, 2024, **12**, 985–993.
17 X. Wang, Y. Wu, X. Wen, J. Zhu, X. Bai, Y. Qi and H. Yang, *Opt. Quantum Electron.*, 2020, **52**, 238.
18 V. Suresh, L. Ding, A. B. Chew and F. L. Yap, *ACS Appl. Nano Mater.*, 2018, **1**, 886–893.
19 L. C. Heng, T. C. Hung and L. D. Zheng, *Spectrochim. Acta, Part A*, 2024, **306**, 123563.
20 O. Prakash, T. Abhijith, G. R. Umapathy, S. Karak, U. B. Singh and S. Ghosh, *Opt. Mater.*, 2024, **148**, 114814.
21 L. L. Qu, N. Wang, G. Zhu, T. P. Yadav, X. Shuai, D. Bao, G. Yang, D. Li and H. Li, *Talanta*, 2018, **186**, 265–271.
22 H. Y. Wu, H. C. Lin, Y. H. Liu, K. L. Chen, Y. H. Wang, Y. S. Sun and J. C. Hsu, *Molecules*, 2022, **27**, 6755.
23 Z. Zhou, S. Zhang, Y. Zhang, M. Xu and C. Xue, *Mater. Sci. Semicond. Process.*, 2024, **179**, 108522.
24 R. Oliveira and A. C. Sant'Ana, *Chemosphere*, 2023, **338**, 139490.
25 Y. Zhao, G. Chen, Y. Du, J. Xu, S. Wu, Y. Qu and Y. Zhu, *Nanoscale*, 2014, **6**, 13754–13760.
26 N. Zhang, L. Tong and J. Zhang, *Chem. Mater.*, 2016, **28**, 6426–6435.
27 B. Zhao, H. Liu, L. Xia, Z. Wang and C. Zhang, *ACS Appl. Nano Mater.*, 2022, **5**, 15341–15352.
28 M. Zhang, H. Sun, X. Chen, H. Zhou, L. Xiong, W. Chen, Z. Chen, Z. Bao and Y. Wu, *J. Alloys Compd.*, 2021, **864**, 158189.
29 L. T. Q. Xuan, L. N. Nguyen and N. T. Dao, *Nanotechnology*, 2022, **33**, 105603.
30 S. Wannapop and A. Somdee, *Ceram. Int.*, 2020, **46**, 25758–25765.
31 C. Shi, M. Eqi, J. Shi, Z. Huang and H. Qi, *J. Colloid Interface Sci.*, 2023, **650**, 1736–1748.
32 S. Y. Lee, H. T. Do and J. H. Kim, *Appl. Surf. Sci.*, 2022, **573**, 151383.
33 N. T. Huyen, T. A. S. Suong, C. T. Thanh, N. V. Tu, P. V. Trinh, T. V. Tan, L. T. Q. Xuan, B. H. Thang, T. V. Hau, D. Tuan, P. D. Long, P. N. Minh, H. Abe and N. V. Chuc, *RSC Adv.*, 2025, **15**, 10754.
34 C. T. Thanh, N. T. Huyen, V. T. Thu, P. V. Trinh, N. V. Tu, B. H. Thang, T. V. Hau, D. Tuan, M. T. Phuong, P. T. Binh, P. N. Minh, H. Abe and N. V. Chuc, *Mater. Lett.*, 2025, **386**, 138209.
35 Y. Wen, H. Ding and Y. Shan, *Nanoscale*, 2011, **3**, 4411–4417.
36 C. T. Thanh, N. T. Huyen, P. V. Trinh, N. V. Tu, V. T. Thu, V. C. Tu, D. N. Nhiem, P. T. Binh, N. N. Anh, V. X. Hoa, P. N. Minh, H. Abe and N. V. Chuc, *Diamond Relat. Mater.*, 2025, **152**, 111889.
37 M. Ilitut, C. Leordean, V. Canpean, C.-M. Teodorescu and S. Astilean, *J. Mater. Chem. C*, 2013, **1**, 4094.
38 V. Vinesh, A. R. M. Shaheer and B. Neppolian, *Ultrason. Sonochem.*, 2019, **50**, 302–310.
39 S. Ghasemi, S. J. Hashemian, A. A. Alamolhoda, I. Gocheva and S. Rahman Setayesh, *Mater. Res. Bull.*, 2017, **87**, 40–47.
40 X. Zhao, W. Wang, Y. Liang, J. Fu, M. Zhu, H. Shi, S. Lei and C. Tao, *Sens. Actuators, B*, 2019, **279**, 313–319.
41 M. Sakir, E. Yilmar and M. S. Onses, *Microchem. J.*, 2020, **154**, 104628.
42 Y. Yang, J. Shi, G. Kawamura and M. Nogami, *Scr. Mater.*, 2008, **58**, 862–865.
43 O. Petruš, J. Macko, R. Oriňaková, A. Oriňak, E. Múdra, M. Kupková, Z. Farka, M. Pastuch and V. Socha, *Spectrochim. Acta, Part A*, 2021, **249**, 119322.
44 X. Jiang, D. Yin, M. Yang, J. Du, W. Wang, L. Zhang, L. Yang, X. Han and B. Zhao, *Appl. Surf. Sci.*, 2019, **487**, 938–944.
45 T. B. Pham, T. H. C. Hoang, V. H. Pham, V. C. Nguyen, T. V. Nguyen, D. C. Vu, V. H. Pham and H. Bui, *Sci. Rep.*, 2019, **9**, 12590.
46 X. Y. Wang, W. Y. Zhang, Y. J. Hu, H. Y. Song, A. Zeeshan, C. Ge and S. B. Liu, *Spectrochim. Acta, Part A*, 2024, **310**, 123932.
47 G. L. Long and J. D. Winefordner, *Anal. Chem.*, 1983, **55**, 712A–724A.
48 K. Wang, D.-W. Sun, H. Pu and Q. Wei, *Analyst*, 2020, **145**, 1801–1809.
49 E. Cara, L. Mandrile, F. F. Lupi, A. M. Giovannozzi, M. Dialameh, C. Portesi, K. Sparnacci, N. D. Leo, A. M. Rossi and L. Boarino, *Sci. Rep.*, 2018, **8**, 11305.
50 W. Chen, W. Wang, H. Xing, W. Li, H. He, W. Li, P. K. Chu, G. Song, H. Wang and P. Li, *Surf. Interfaces*, 2023, **38**, 102808.
51 Y. Liu, R. Li, N. Zhou, M. Li, C. Huang and H. Mao, *Appl. Surf. Sci.*, 2022, **582**, 152336.
52 L. Mei, Z. Wang, Y. Niu, W. Deng and Y. Shao, *Opt. Express*, 2023, **31**, 29768.
53 H. Zhai, C. Zhu, X. Wang, Y. Yan and H. Tang, *Front. Chem.*, 2022, **10**, 992236.
54 S. Kumar, D. K. Lodhi and J. P. Singh, *RSC Adv.*, 2016, **6**, 45120.

55 X. Chong, B. Zhao, R. Li, W. Ruan and X. Yang, *Colloids Surf., A*, 2015, **481**, 7–19.
56 Y. Wang, M. Zhang, H. Yu, Y. Zuo, J. Gao, G. He and Z. Sun, *Appl. Catal., B*, 2019, **252**, 174–186.
57 P. Midya, P. P. Sarngan, A. Dutta, K. K. Chattopadhyay and D. Sarkar, *Mater. Sci. Eng., B*, 2022, **286**, 116028.
58 M. R. Al-Mamun, M. N. Karim, N. A. Nitun, S. Kader, M. S. Islam and M. Z. H. Khan, *Environ. Technol. Innovation*, 2021, **22**, 101537.
59 Y. Chen, Y. Tang, S. Luo, C. Liu and Y. Li, *J. Alloys Compd.*, 2013, **578**, 242–248.
60 W. Zhai, M. Cao, Z. Xiao, D. Li and M. Wang, *Foods*, 2022, **11**, 3597.
61 K. V. Serebrennikova, N. S. Komova, A. V. Aybush, A. V. Zherdev and B. B. Dzantiev, *Materials*, 2023, **16**, 1475.
62 C. K. Mitra, M. D. Sharma, M. Ghosh, S. Pande and J. Chowdhury, *Curr. Appl. Phys.*, 2024, **63**, 18–21.
63 R. Sinha, S. K. Das, M. Ghosh and J. Chowdhury, *Front. Chem.*, 2022, **10**, 1034060.
64 A. Averkiev, R. D. Rodriguez, M. Fatkullin, A. Lipovka, B. Yang, X. Jia, O. Kanoun and E. Sheremet, *Sci. Total Environ.*, 2024, **935**, 173262.
65 Y. Vasseghian, E. N. Dragoi, F. Almomani, N. Golzadeh and D. V. N. Vo, *Chemosphere*, 2022, **291**, 132789.
66 A. M. Al'Abri, S. N. Abdul Halim, N. K. Abu Bakar, S. M. Saharin, B. Sherino, H. Rashidi Nodeh and S. Mohamad, *J. Environ. Sci. Health, Part B*, 2019, **54**, 930–941.